REVIEW ARTICLE

Investigation of non-collinear spin states with scanning tunneling microscopy

W Wulfhekel[1] and C L Gao[2]

[1] Physikalisches Institut, Universität Karlsruhe (TH), Wolfgang-Gaede Straße 1,
76131 Karlsruhe, Germany
[2] Max-Planck Institut für Mikrostrukturphysik, Weinberg 2, 06120 Halle, Germany

E-mail: w.wulfhekel@pi.uni-karlsruhe.de

Abstract
Most ferromagnetic and antiferromagnetic substances show a simple collinear arrangement of
the local spins. Under certain circumstances, however, the spin configuration is non-collinear.
Scanning tunneling microscopy with its potential atomic resolution is an ideal tool for
investigating these complex spin structures. Non-collinearity can be due to topological
frustration of the exchange interaction, due to relativistic spin–orbit coupling or can be found in
excited states. Examples for all three cases are given, illustrating the capabilities of
spin-polarized scanning tunneling microscopy.

(Some figures in this article are in colour only in the electronic version)

1. Introduction

Magnetism on the nano-scale has been in the focus of intensive research in the past decades due to its relevance for high-density magnetic recording, magnetic random-access memory and magnetic sensors [1–4] as well as due to many fundamental issues regarding the physics spin systems. A detailed knowledge of the spin structure on the atomic level of magnetic nano-structures is helpful in understanding their magnetic properties as well as interactions like the exchange bias. Most ferromagnets, ferrimagnets as well as antiferromagnets display relatively simple collinear spin structures in which the atomic moments point along one well-defined axis. This ground state configuration is mostly due to the Heisenberg exchange interaction $J_{ij}\vec{S}_i \cdot \vec{S}_j$ between neighboring spins $\vec{S}_i$ and $\vec{S}_j$ either favoring a parallel or antiparallel orientation depending on the sign of the exchange J_{ij} [5]. In these structures, the electrons, which give rise to the atoms magnetic moment, can be divided into majority and minority spin states such that the magnetic state of the system is described by the population of the electrons in the two spin states.

Traditional methods to study magnetism on the atomic level are usually bulk sensitive like neutron diffraction [6, 7] and operate in reciprocal space. As to thin films, magnetic x-ray linear dichroism can map the magnetization direction in ferromagnets or magnetization axis in antiferromagnets [8], and scanning electron microscopy with polarization analysis has been used to resolve magnetic structures [9]. While they operate in real space, they are, however, limited in lateral resolution and cannot resolve the atomic spin structures that are of interest, here. Only with the development of spin-polarized scanning tunneling microscopy (Sp-STM), it is possible to map the spin configuration of the surface on the atomic level [10]. This opens up the possibility to study even complex spin structures in real space, as will be reviewed in this work.

While collinear spin structures are common, they are not the only solution to the simple exchange dominated spin structures. In some crystal structures, an antiferromagnetic exchange between nearest neighbors cannot be fully satisfied due to topological reasons such that the ground state is a non-collinear state. A prototypic example for such a system is the antiferromagnetic two-dimensional hexagonal lattice [11]. In this lattice it is topologically impossible to align the spins within any triangle of nearest neighbors in an antiparallel fashion. Instead, a frustrated antiferromagnetic Néel structure is stabilized. Here, the magnetic moments are aligned with an angle of 120° between neighboring magnetic moments. With rising crystal complexity, these non-collinear states are

more probable. As a consequence, the electronic state cannot be fully described by the density of states for minority and majority electrons. Instead, when choosing a quantization axis for the electron spin, the electronic states in the atoms have to be described by a coherent superposition of the two spin states, i.e. the phase between the minority and majority electron states becomes important. As a consequence, a single measurement of the population of the states is insufficient to distinguish between a collinear and a non-collinear spin state. Instead, information containing the phase or the combined measurement of the spin configuration with different quantization axes is required. These spin structures and their determination will be discussed in detail in section 3.

A second class of non-collinear spin states arise from higher order effects involving the spin and orbital moments. While the simple Heisenberg Hamiltonian for the exchange considers the spin $\vec{S}$ of the electrons as a good quantum number, the relativistic spin orbit interaction may lead to mixing of the spin states and as a consequence to non-collinear states. Besides the resulting magnetocrystalline anisotropy, a well-known effect of the spin–orbit interaction in systems with broken inversion symmetry is the anisotropic exchange or Dzyaloshinsky–Moriya interaction [12, 13] leading to an additional exchange of the form $\vec{D}_{ij} \cdot \vec{S}_i \times \vec{S}_j$. This additional term may lead to a non-collinear ground state. Moreover, the spin orbit interaction may as well be a function of the electron energy. As a consequence, the spin of the electronic states may be subject to an energy-dependent mixing such that even within one atom, the spin is non-collinear in the energy domain. Two examples for non-collinearity due to spin–orbit interaction will be discussed in section 4.

So far, we discussed only the magnetic ground state. While this state is of utmost importance for the description of static properties of the magnetic system, it does not describe the states at finite temperatures or its dynamics. Instead, one needs to investigate a third class of non-collinear states, the elementary excitations of magnetic systems. In the Heisenberg description of magnetism, the elementary excitations are collective excitations of the local magnetic moments in the form of spin waves or magnons. These excitations travel through the crystal as a periodic wave, in which the individual magnetic moments precess around their ground state direction, i.e. the excited state is a non-collinear state even in simple ferromagnets. In section 5, we will show how these states can be investigated.

2. Spin-polarized scanning tunneling microscopy

With the development of Sp-STM, a real space imaging technique is at hand that enables to explore the magnetic structure down to atomic level, to verify the theoretical predictions, and to put many phenomenological models on a solid microscopic base.

In conventional scanning tunneling microscopy (STM), the electrons that tunnel between the tip and the conductive surface are used as a feedback parameter to position the tip. During scanning in the constant current mode, the apex of the tip is held on several Å above the sample surface by the

feedback mechanism. In the Tersoff–Hamann model [14, 15], the constant current correspond to positioning the tip at constant local density of states (LDOS) of the sample surface. Maps of the vertical tip position are called topographic STM images while they reflect the spatial distribution of the LDOS of the electrons [16]. When a tip with an atomically sharp apex is used, individual atoms can be resolved [17]. In the above picture, the spin of the electron has been neglected. For magnetic atoms the density of states is, however, spin-split into majority and minority states and a net imbalance between the occupation of both leads to the magnetic moment. In Sp-STM the tip itself is spin-polarized. Information on the spin polarization of the sample surface may be obtained via the spin-dependent tunneling process between tip and sample as described in the following.

2.1. Spin-polarized tunneling

The principle of operation of Sp-STM is based on the imbalance of the LDOS of different spins. The imbalance causes a spin polarization $\vec{P}$ of the LDOS that has immediate consequences on the tunneling current as discovered by Jullière [18]. When electrons tunnel between two ferromagnets, the magnitude of the current is influenced by the magnetization of the two electrodes, or to be more precise, the junction resistance depends on the relative orientation of the spin polarizations $\vec{P}_1$ and $\vec{P}_2$ of the electrodes. This effect was therefore named the tunneling magnetoresistance (TMR) effect. For parallel orientation of the spin polarizations, the conductance G is higher than for antiparallel orientation. This finding has been explained on basis of a simple model for tunneling in which we neglect any spin dependence in the transmission through the barrier as well as spin-flip scattering during the tunneling process [19]. A quantum mechanical treatment of the problem of spin-polarized tunneling for arbitrary angles θ between the two spin polarizations leads to:

$$G = G_0(1 + \vec{P}_1 \cdot \vec{P}_2) = G_0(1 + P_1 P_2 \cos\theta) \qquad (1)$$

where $|\vec{P}_i| = (N_{i\uparrow} - N_{i\downarrow})/(N_{i\uparrow} + N_{i\downarrow})$ is the spin polarization of the LDOS of the electrode i given by the LDOS N_i for majority $\uparrow$ and minority $\downarrow$ electrons. Here G_0 depends on the bias voltage and the tip sample separation but not on the spins. This prediction was later experimentally confirmed [20].

If a finite bias is applied, all states between the Fermi levels of the electrodes are involved in tunneling and have to be weighted according to their tunneling probability. This scenario is more complex but G can be expressed using effective spin polarizations.

2.2. The imaging modes of Sp-STM

In Sp-STM a spin-polarized tip (magnetic or antiferromagnetic) is used to map the magnetic surface. As in an STM experiment, the tunneling current is also used to extract information of the electronic density, one needs to separate magnetic and non-magnetic information in the tunneling current to image topographic and magnetic properties of the sample surface. There were several modes proposed to achieve this [21]. We here use two modes, which will be discussed in the following.
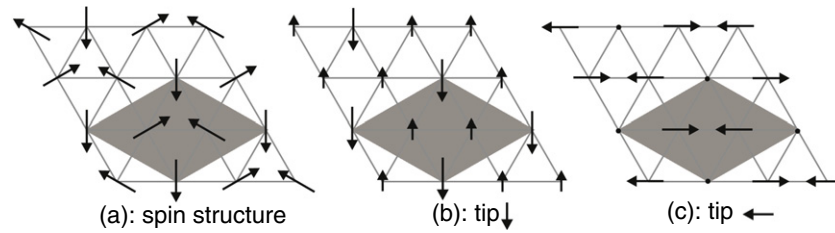
(a): spin structure   (b): tip↓   (c): tip ←

Figure 1. 120° Néel antiferromagnetic structure in a hexagonal lattice (a) and the projection of the spin polarizations on the axis parallel (b) and perpendicular (c) to one atomic moment. The magnetic unit cell is indicated by the gray diamond.

2.2.1. The constant current mode. Identical to STM, in the constant current mode of Sp-STM, the surface is scanned in the constant current mode but with a spin-polarized tip. Due to the TMR effect, the conductivity also depends on the projection of the sample spin polarization on the spin polarization of the tip such that a mixture of topographic and spin information is contained in the Sp-STM images. Sample areas with a spin polarization parallel to that of the tip appear higher while areas with antiparallel spin polarization appear lower. Ultimately, atomic resolution in spin has been obtained on flat surfaces. The reason for the high spin resolution with magnetic tips has been explained on basis of the magnetic super cell being larger than the structural unit cell [22]. Thus, the translational symmetry is lowered resulting in a significantly slower decay of the surface magnetic corrugation than the atomic corrugation. This is due to a longer wavelength of the magnetic structures in real space. These components are closer to the center of the surface Brillouin zone and thus decay slower into the vacuum than the structural components that are far out in the surface Brillouin zone. A constant current image taken with a magnetic tip on a flat substrate therefore reflects the magnetic super cell rather than the atomic unit cell. The magnetic contribution in the constant current Sp-STM image is proportional to the projection of the spin polarization of the sample on the spin polarization of the tip [22]. Sp-STM operating in the constant current mode has demonstrated its ultimate resolution in many two-dimensional antiferromagnetic systems, such as Fe/W(001) [23] and Mn/W(110) [24].

2.2.2. The differential magnetic mode. In the differential magnetic imaging mode, a magnetically bistable bulk ferromagnetic tip is used whose magnetization is periodically switched between opposite magnetization directions [25]. This is equivalent to changing the sign of the spin polarization of the tip. The switching frequency of the alternating current lies above the cut-off frequency of the feedback loop of the STM such that the feedback loop only detects the averaged tunneling current. As can easily be seen from equation (1), in the time averaged tunneling current all spin-dependent currents cancel out such that the topographic image contains no magnetic information. With a phase-sensitive lock-in amplifier, the alternating part of the tunneling current is detected which is proportional to $\vec{P}_1 \cdot \vec{P}_2$ containing exclusively spin information. This way, topographic and spin information are strictly separated. Depending on the shape of the tip, the

out-of-plane as well as the in-plane component of the sample spin polarization can be mapped [25, 26]. The advantage of the differential magnetic mode is that the electronic structure of the sample may be arbitrary and even varying and still the spin polarization can be measured. For a more detailed description of the imaging modes, read a recent review [27].

3. Frustrated states

As discussed in section 1, frustration of antiferromagnetic order can be due to the topological structure of the lattice of antiferromagnetic atoms. Due to competing exchange interactions between neighboring atoms, non-collinear frustrated spin structures are formed, which play an important role in determining the exchange bias at the interface between ferromagnets and the many non-collinear antiferromagnets [28]. Therefore, the investigation of non-collinear spin structures is both of fundamental interest and of technological importance [29]. Two examples will be discussed. First, the prototypic two-dimensional hexagonal antiferromagnetic lattice will be presented in form of a single atomic layer of Mn on the hexagonal surface of fcc Ag(111). Second, the surface spin structure of a complex three-dimensional antiferromagnet in the case of α-Mn grown on Fe(001) will be discussed.

3.1. Hexagonal antiferromagnets: Mn/Ag(111)

The classical example of non-collinear antiferromagnetic spin structure is an arrangement of antiferromagnetic atoms in a two-dimensional hexagonal lattice. In this lattice it is impossible to align all nearest neighbors antiparallel such that rather a frustrated antiferromagnetic Néel structure as shown in figure 1(a) is stabilized. In this case, the magnetic moments are aligned with an angle of 120° between neighboring magnetic moments.

A two-dimensional hexagonal arrangement of antiferromagnetic atoms is usually realized by growing a monolayer (ML) of magnetic atoms on the hexagonal (0001) surfaces of hcp or (111) surfaces of fcc crystals. Depending on the details of the exchange interaction, spin structures from row-wise antiferromagnetic, double-row-wise antiferromagnetic or non-collinear 120° Néel alignment have been predicted [30–34]. It has been proposed by Wortmann *et al* [22] that using Sp-STM operating in the constant current mode, the collinear and non-collinear antiferromagnetic spin structures of a monolayer
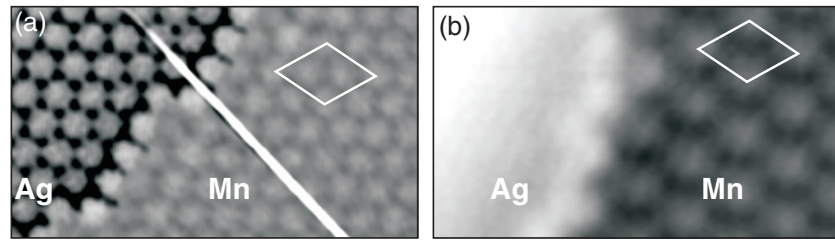
Figure 2. High resolution STM images taken at 5 K with a non-magnetic W tip (a) and a magnetic Cr tip (b) close to a Ag(111) step edge decorated with Mn. In (a), the fcc stacking of Ag and Mn is visible. In (b), magnetic unit cell is resolved on Mn while no atomic feature is resolved on Ag. The size of magnetic unit cells is marked on both images. The size of the images is about 3.5 nm × 2 nm.

two-dimensional antiferromagnet on fcc(111) surfaces can be distinguished experimentally. The magnetic contribution in the constant current Sp-STM image is proportional to the projection of the spin polarization of the sample on the spin polarization of the tip. In the case of the non-collinear Néel structure in figure 1(a), the projection of the magnetic moments on two orthogonal orientations as shown in figure 1(b) (the magnetization direction of the tip parallel to one of the moments) and 1(c) (the magnetization direction of the tip perpendicular to one of the moments) results in different Sp-STM images showing both a magnetic ($\sqrt{3} \times \sqrt{3}$) super cell [22].

As a model system Mn on Ag(111) was investigated. Sub-monolayer deposition of Mn on clean Ag(111) single crystals at substrate temperatures of 200 K leads to pseudomorphic growth of single ML high Mn islands without intermixing between Mn and Ag [35]. The Mn either grows as triangular islands or along the Ag step edges forming ML stripes. In the former case, the islands can be of fcc or hcp stacking. In the latter case, atomically resolved topographic images with non-magnetic tips (see figure 2(a)) show that the Mn continues the fcc stacking of the Ag substrate without dislocations at the step edge.

For magnetic measurements, the W tips were coated with ≈70 ML of Cr which gives an in-plane spin sensitivity [36]. Sp-STM images of a Mn decorated Ag step are shown in figure 2(b). On the Ag terrace, no spin contrast is observed while on the Mn film, a clear ($\sqrt{3} \times \sqrt{3}$) super cell emerges, that is absent in topographic images recorded with non-magnetic tips. The symmetry of the unit cell is not consistent with a row-wise or double-row-wise antiferromagnetic state but only agrees with a non-collinear 120° Néel alignment. With one measurement, however, a non-collinear structure cannot be strictly proven. Thus, measurements of the very same area of the sample but with different tip magnetization directions are required. In case the spin structure is collinear, the observed Sp-STM images should all be identical except for the exact size of the magnetic contrast, while the non-collinear case is indicated by different Sp-STM patterns of the unit cell.

Considering the hexagonal 120° Néel structure of a ML of Mn and assuming a spin direction along a high symmetry direction, only four energetically degenerate domains exist as sketched in figure 3(a). Note that a rotation of all spins by 120° is equivalent to a translation by a lattice vector and that patterns I and IV as well as patterns II and III are related by a rotation of all spins by 60°. If these spin structures are now imaged with a spin-polarized tip, four different images result.
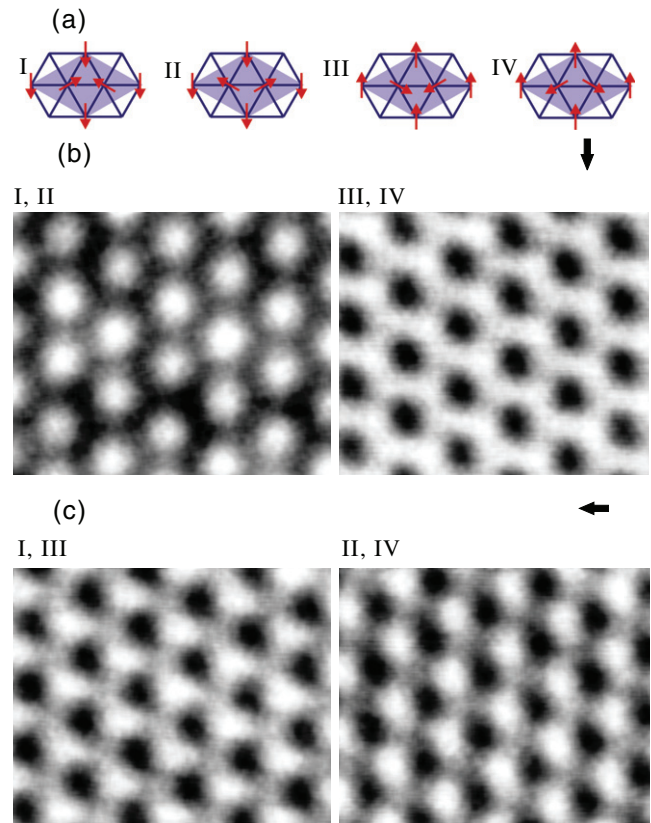

Figure 3. (a) Four possible configurations of the 120° Néel structure (modulo a 120° rotation of all spins in the same sense). (b) and (c) are two groups of constant current images taken with magnetic tips. The size of the images is about 2 nm × 2.5 nm. The magnetic unit cells are marked in the images together with the projection of the sample spin polarization onto the tip spin polarization direction. By assuming a magnetic orientation of the tip, the projections of the four domains in (a) on the tip magnetization direction results in different magnetic images. All images were taken on two fcc stacked islands.

If the tip spin polarization is parallel to that of one of the Mn atoms (say the top one), the projection of domain I and II on the tip spin polarization direction give identical images. The top atom appears brighter and the two other atoms within the unit cell have a smaller projection onto the tip polarization and appear darker. A reversal of all spins of the structure leads to an inversion of the contrast. Due to the symmetry properties of the projections, in both cases a pattern of six-fold rotational symmetry arises. These structures have been experimentally
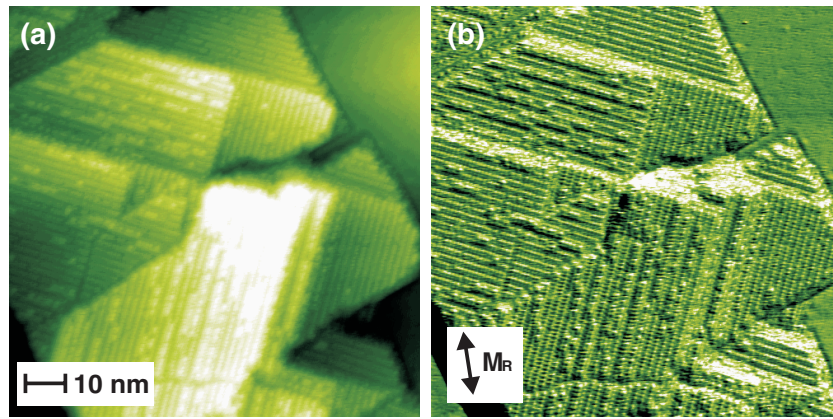
Figure 4. Sp-STM images of (a) the topography and (b) the spin signal of 12 ML Mn on Fe(001) ($U = 0.1$ V, $I = 3$ nA). The atomically flat terraces are bct Mn while the rough island is α-Mn. The spin structure of the first is homogeneous while that of the islands show a complex structure. M_R shows the magnetization direction of the ring.

observed on top of fcc islands as shown in the left and right image of figure 3(b).

If the tip spin polarization is perpendicular to one of the Mn moments, the three atoms in the unit cell give three different projections of their spin polarization on the tip spin polarization thus leading to patterns of only three-fold rotational symmetry. These can also be observed on the same islands in case a small amount of Cr was removed from the tip with voltage pulses altering the in-plane spin polarization of the tip (see figure 3(c)). As these images are of a lower rotation symmetry, they are are not proportional to the six-fold symmetric ones proving a non-collinear Néel structure.

The above discussion of fcc Mn layers can also be carried out for the hcp stacked regions, were also a 120° Néel structure was found [35]. However, a different magnetic anisotropy for fcc and hcp islands was observed stemming from the different spin–orbit coupling with the Ag substrate. It could be shown that the Mn moments rotate by 30° when going from a fcc to a hcp stacked region.

3.2. Complex antiferromagnets: Mn/Fe(001)

Manganese has the most complex structural and magnetic properties among all elements. At room temperature, Mn shows a non-collinear antiferromagnetic structure in its α-Mn phase [6, 7] which has a body centered cubic structure of 58 atoms in the unit cell. Simpler phases of Mn were obtained by growing Mn on the surface of other materials [37, 38]. Due to the influence of the substrate lattice, Mn could be stabilized on Fe(001) in a body centered tetragonal (bct) structure. While Mn grows in a layer-by-layer fashion pseudomorphically on Fe(001) [37] showing a layer-wise antiferromagnetic structure [39–41] for the first ≈12 ML, the flat growth changes to a three-dimensional growth, above [42]. It was proposed that the change of the growth mode is accompanied by a structural transition from the simple bct Mn to the complex α-Mn.

Mn films on Fe(001) were investigated in the differential magnetic imaging mode using ring shaped electrodes as STM tips. These electrodes have a well-defined in-plane spin polarization [26]. In the transition region, the bct Mn and reconstructed Mn coexist as shown in figure 4(a). In the topographic image, part of the surface is atomically flat bct Mn (see upper right corner). In the corresponding spin channel figure 4(b), a homogeneous contrast is observed in that region. The ring was arranged parallel to the magnetization direction of the Fe(001) whisker such that the constant spin contrast reflects the collinear alignment of the bct Mn magnetization to that of the Fe whisker [43]. Most of the image, however, shows a reconstructed three-dimensional island. On the top of the island, periodic features could be observed in topography. Obviously, the reconstruction to the α-Mn starts as islands. In the spin channel (cf figure 4(b)), orthogonal crystallographic domains of a regular contrast are seen, suggesting that the reconstructed Mn shows a complex magnetic structure.

As suggested by low energy electron diffraction (LEED) as well as topographic STM images, the reconstruction has a unit cell size of 9 Å by 18 Å, i.e. it is twice as large as the unit cell of the (001) surface of α-Mn. From this point of view, the reconstructed Mn has the symmetry of a p(2×1) reconstruction of α-Mn. The reconstruction is characterized by parallel lines of protrusions, which are separated by 18 Å. According to both LEED and STM, four sub patterns with lines parallel running along [130], [$\bar{1}$30], [310] and [$\bar{3}$10] directions coexist.

The spin configuration within the unit cells of the reconstruction was visible when zooming into those islands. Figures 5(a) and (b) show the spin images of two structural domains with perpendicular orientations of the reconstruction lines. The sensitive direction of the tip is indicated in both. Note that the two images were cut from one larger image to ensure identical tip conditions. Interestingly the images differ. This can be explained by the fact that the two images represent the same unit cell but imaged with different relative orientations between the unit cell and the tip spin polarization, i.e. in figure 5(a) $\vec{P}$ is almost parallel to the long edge of the unit cell while it is nearly perpendicular in figure 5(b). As the two unit cells are identical except for their rotation, this implies that the two orthogonal components of the spin polarization within the unit cell show different patterns, i.e. the spin polarization is non-collinear. The non-collinear spin
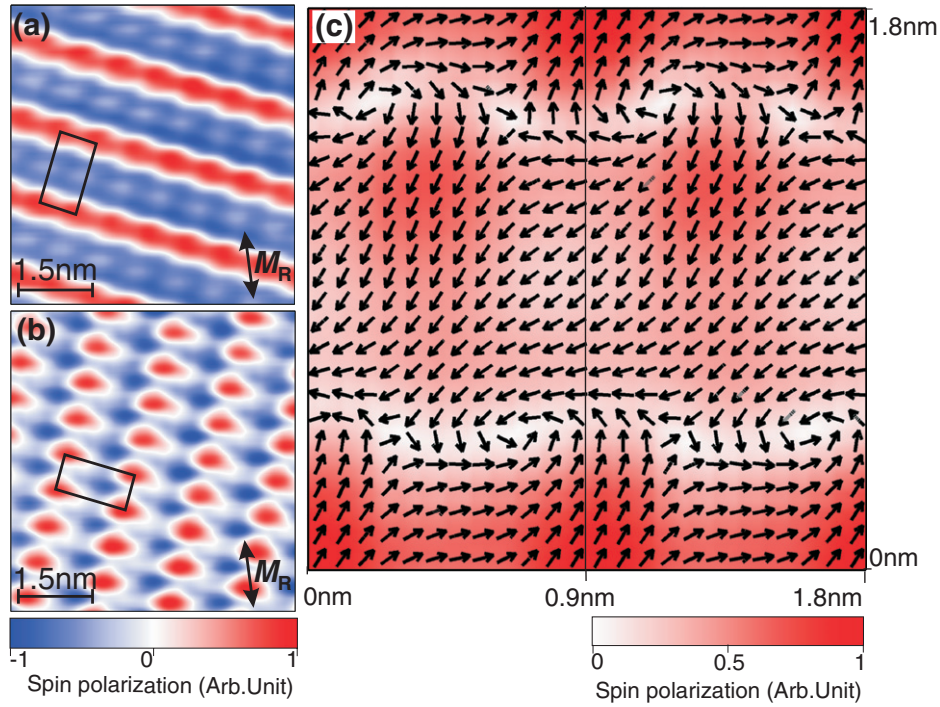
Figure 5. (a), (b) Spin images taken on top of two domains of the reconstructed Mn of orthogonal orientation ($U = 0.10$ V, $I = 3$ nA). The unit cell of 9 Å × 18 Å is indicated in the images. M_R shows the magnetization direction of the ring. (c) gives the vector spin distribution of the reconstruction (two unit cells are shown) by combining image (a) and (b).

structure of the reconstructed Mn surface is not surprising since the surface structure is similar to a doubled bulk α-Mn structure while bulk α-Mn has a complex non-collinear spin structure [7]. Since the two domains are perpendicular to each other, the two spin images can be combined to give a two-dimensional spin distribution map as shown in figure 5(c). The image shows the relative magnitude of the spin polarization within the unit cell, while the arrows represent their directions. Though this spin map is not in atomic scale, it does reveal a complex non-collinear structure of the reconstructed α-Mn surface with vortex and antivortex structures in the unit cell. Only due to the well-defined direction of the tip spin polarization, the two images can be combined to a vector map. In case the direction of the tip spin polarization is not known, vector maps can only be constructed modulo an arbitrary angle of rotation of the spins, in which case vortices and antivortices cannot be distinguished.

4. Non-collinear states due to spin–orbit interaction

While in the absence of spin–orbit interaction the spin $\vec{S}$ of the electron is a conserved quantity, in any solid state structure the spin feels the crystal environment by the spin–orbit interaction and the eigenstates of the electrons are not pure spin states but are rather mixed. One of the most important consequences is the appearance of the magnetocrystalline anisotropy in magnets, i.e. the dependence of the energy of the magnetic system on the direction of magnetization. In point symmetric structures the energy of the magnetic system must depend on the magnetization direction in a point symmetric fashion.

Thus, easy axis of magnetizations evolve, in which the energy of the magnet is identical for $\vec{M}$ and $-\vec{M}$.

4.1. Anisotropic exchange: Mn/W(110)

In case the inversion symmetry is broken, there is, however, no reason that the spin–orbit interaction conserves inversion symmetry. Especially in thin films, the inversion symmetry is broken, as the film is supported by a substrate from below and has vacuum above. This maximal breaking of inversion symmetry in combination with a heavy substrate, i.e. a substrate with large spin–orbit interaction, may lead to a significant anisotropic exchange interaction [12, 13] that dominates the ground state spin structure [24].

The single ML of Mn on the pseudohexagonal surface of W(110) was shown to have a row-wise antiferromagnetic order with magnetic moment pointing along the [110] and [$\overline{1}$10] direction [10]. A constant current image using an in-plane sensitive Cr coated W tip shows that the Mn grows pseudomorphically and flat on the W substrate (cf figure 6(a)) but also the presence of large scale magnetic contrast within the island. Zoomed images reveal a row-wise antiferromagnetic contrast visible as vertical lines of spin-related corrugations (see figure 6(b)). Interestingly, superimposed on the row-wise contrast there is a large scale periodic modulation of the contrast. As shown in the line scans of figure 6(c), the spin-related contrast oscillates with atomic distances and is modulated by a 6 nm modulation. Note that the atomic modulation changes signs when going through a node of the large scale modulation. This spin structure could be related to
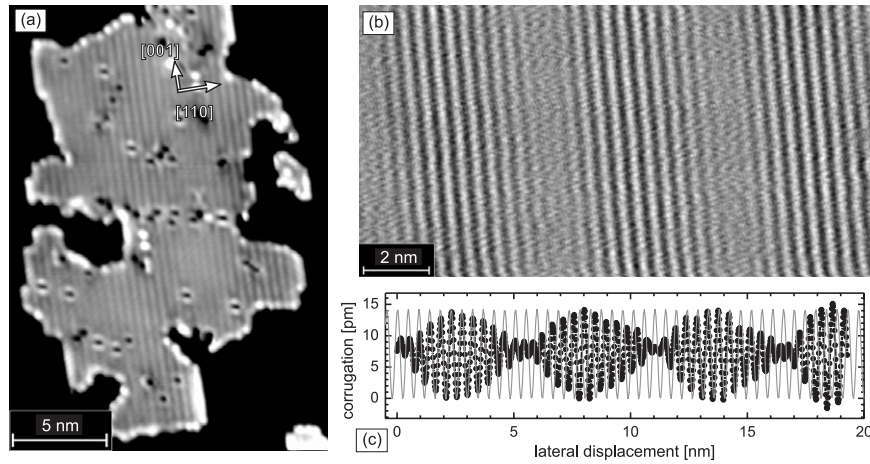
Figure 6. (a) Sp-STM images of a 1 ML Mn island on W(110) recorded with an in-plane polarized Cr coated W tip. (b) Zoom into the magnetic structure showing a large scale modulation of contrast on top of the row-wise antiferromagnetic contrast. (c) Height profile of the Sp-STM scan across the non-collinear spin structure.
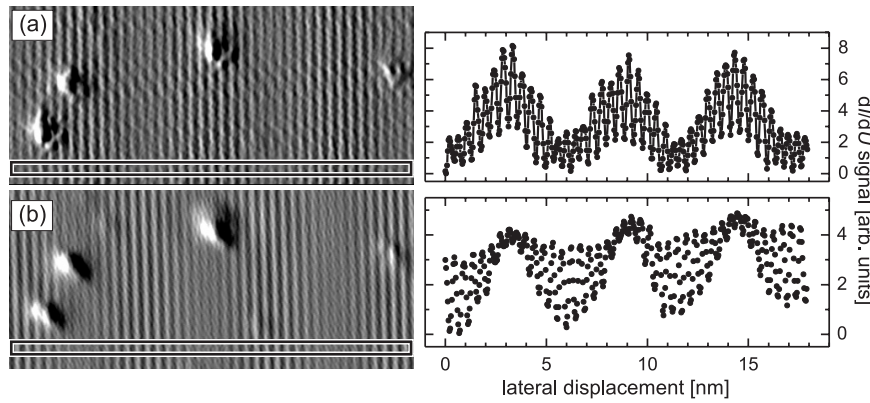

Figure 7. 1 ML Mn on W(110) imaged in the constant current mode using an Fe coated W tip. By applying a magnetic field perpendicular to the sample surface, the tip magnetization is progressively reoriented from an in-plane direction (a) to a nearly out-of-plane state (b).

a spin density wave, i.e. a collinear modulation of the size of the spin polarization, or to a non-collinear spin spiral.

To distinguish between the two, measurements of different direction of sensitivity need to be obtained. This can be achieved by using Fe coated W tips and applying a large magnetic field to align the tip spin polarization. As shown in figure 7, the very same sample area was scanned with an Fe coated tip while varying an external magnetic field perpendicular to the sample surface. Assuming that the spin structure of the antiferromagnetic Mn film is not changed by the moderate magnetic fields and realizing that the magnetization of the Fe tip progressively aligns with the rising magnetic field, both an in-plane and out-of-plane spin images can be obtained. Interestingly, the observed Sp-STM images of the sample change with the application of the magnetic filed. The areas of maximal corrugation move laterally excluding a spin density wave and implying that the spin structure is a non-collinear spiral. *Ab initio* calculations including the spin–orbit interaction indicated that the ground state of Mn on W(110) indeed is a cycloidal spin spiral with a spiral periodicity of 8 nm in good agreement with the experiment [24].

4.2. Intra-atomic non-collinear spin density: NiMn/Cu(001)

As the spin–orbit interaction only conserves the total angular momentum $\vec{J} = \vec{L} + \vec{S}$, the eigenstates of the magnetic atom in presence of the spin–orbit interaction are not pure states regarding $\vec{S}$ but are rather coherent superpositions. In the extreme case, this may lead to a spin polarization $\vec{P}(E)$ within the atom, which is non-collinear. This non-collinearity of the electronic states is often neglected, as Hunds rule predicts collinear spin states in which even the orbital momentum $\vec{L}$ and the spin $\vec{S}$ are parallel or antiparallel.

Under certain circumstances, however, the mixing of spin states is pronounced. This can be the case if two electronic bands of opposite spins cross. Within perturbation theory, the spin–orbit interaction leads to an avoided level crossing opening a small gap. Additionally, the spin character of the bands continuously varies between minority and majority at the avoided crossing. Such an effect can be of importance especially in layer-wise antiferromagnets, as in their case, minority and majority bands are in principle degenerate. This is a consequence of the spin structure, as a translation of the magnetic structure by one crystallographic unit vector is
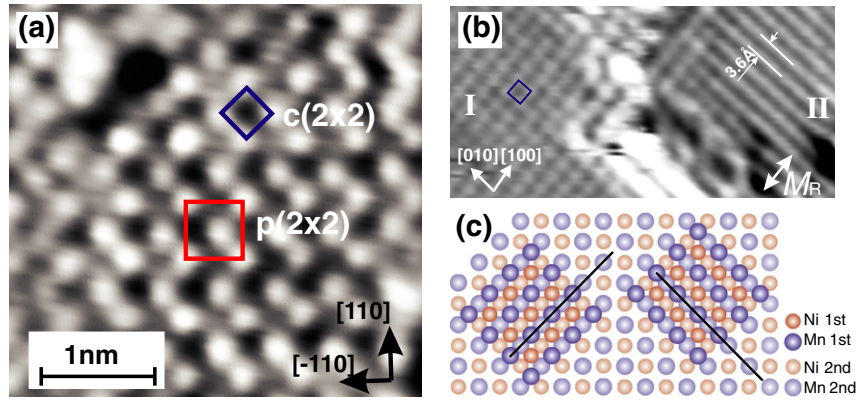
Figure 8. (a) Topographic image of 15 ML NiMn on Cu(001) taken with a STM tip and (b) Sp-STM image taken in the differential magnetic mode. (c) Model of the two structural domains.

equivalent to the inversion of all spins. Thus the minority and majority bands are degenerate and even moderate spin–orbit interaction can lead to significant mixing of the spin states. As an example, we focus on the chemically ordered $Ni_{50}Mn_{50}$ alloy of CuAu-I face centered tetragonal (fct) structure in which Mn and Ni atoms occupying alternating atomic sheets perpendicular to the c axis. The magnetic moments of adjacent Mn atoms lie within the Mn sheets and are antiparallelly aligned while the Ni moments vanish [44], resulting in a layer-wise antiferromagnetic structure along a or b direction. Chemically ordered equiatomic NiMn can be grown epitaxially on Cu(001) while the c axis lies in the substrate plane [45]. In this configuration, the chemical unit cell naturally results in a c(2×2) structure observed in LEED.

And indeed, bright dots, i.e. the Mn atoms, in the atomically resolved topography obtained by STM clearly form c(2×2) cells (cf square in figure 8(a)). A careful analysis of the STM image shows, however, that the central atom in the larger p(2×2) square slightly shifts from the center towards the right-bottom corner. Further, every second bright Mn atom appears higher (brighter) and every second dark depletion, i.e. Ni atoms, deeper (darker). Both observations are compatible with a larger p(2×2) unit cell and indicate a broken c(2×2) symmetry by surface reconstruction. This reconstruction was also observed in a careful LEED-IV analysis [46] revealing a slight buckling of both the surface Ni and Mn atoms.

Due to the four-fold symmetry of the Cu(001) substrate, two orthogonal domains of NiMn exist. These are distinguished by the orientations of the Mn sheets either along [100] or along [010] directions. Spin-resolved images (cf figure 8(b)) show two different spin patterns (marked as domains I and II). Domain I displays a c(2×2) checkerboard structure while domain II exhibits parallel lines, the separation of which equals that of adjacent Mn sheets. Thus, these spin patterns reflect two structural domains with orthogonal Mn sheets that for symmetry reasons are expected to have identical spin structures. By a detailed study of the behavior of the spin polarization when crossing atomic steps, the two domains could be identified [46] as depicted in figure 8(c).

Due to their 90° rotation, however, two orthogonal components of their spin polarization can be mapped as a function of the bias voltage as depicted in figure 9(a). They depend significantly on the bias voltage. For domain I ($\vec{M}_R$ parallel to the Mn sheets; upper row in figure 9(a)), the spin-resolved image for −0.1 V shows weak contrast with p(2×2) symmetry. At positive voltages, the spin unit cell is reduced to a c(2×2) unit cell. For domain II ($\vec{M}_R$ perpendicular to the Mn sheets; bottom row of figure 9(a)), there is apparently no ordered feature at negative bias voltages. The spin pattern at positive voltages is characterized by parallel stripes separated by 3.6 Å reflecting the two-fold symmetry of the film due to the atomic sheets. This complex behavior indicates firstly a non-collinearity of the spin polarization in real space and secondly, a change of the spin polarization direction as a function of bias voltage. The latter can be viewed as non-collinearity of the spin polarization in the energy domain.

The two sets of data for orthogonal domains can be combined to an in-plane vector map of the spin polarization (see figure 9(b)) showing that both direction and relative magnitude of the spin polarization depend strongly on the bias voltage.

Ab initio calculations of NiMn films indicate that the ground state spin structure of an unreconstructed NiMn surface is collinear. If, however, the geometric symmetry is broken by the observed reconstruction, a non-collinear in-plane magnetic structure that depends on the electron energy evolves caused by spin–orbit interaction [46].

5. Non-collinear excited states

Ferromagnetic and antiferromagnetic systems are part of modern data storage devices. For a functioning device, not only the ground state properties of magnetic materials are of interest. Every time, the device is switched, i.e. when a field is sensed or data is written, a magnetic system is excited. The fundamental excitations of magnets are collective excitations in the form of magnons. Magnons are at the heart of physical properties such as fast magnetization reversal, zero bias anomalies in magnetic tunneling junctions or current induced magnetic switching [47–49].

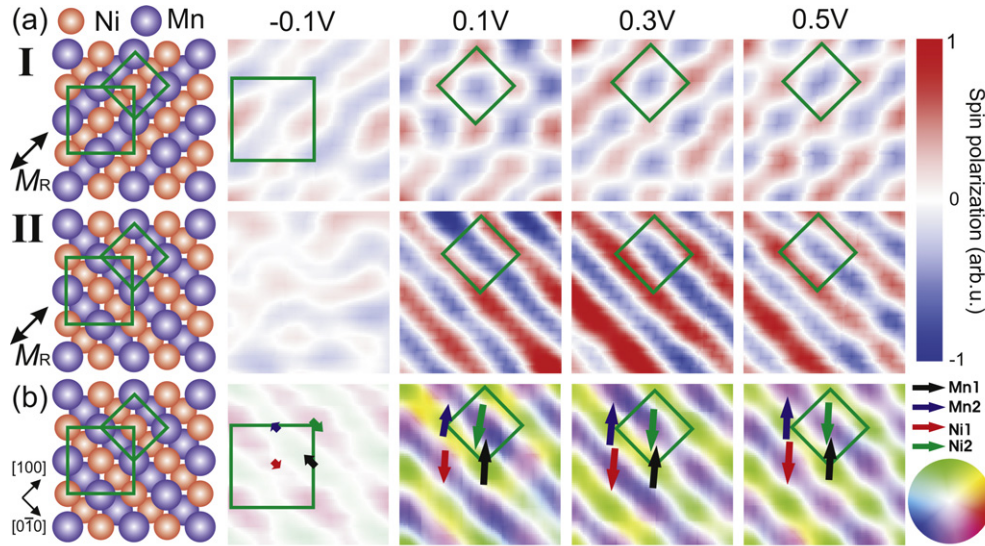Recently, STM has been used to study the energetics of spin-flip scattering in magnetic films, atomic chains, and

Figure 9. (a) Sp-STM images of NiMn for indicated bias voltages of domain I (top row) and domain II (center row). The images (1×1 nm^2) were taken successively at the same spot. (b) Vector plot of the spin polarization, as obtained from the data above. The color wheel gives direction and relative magnitude (increasing radially) of the spin polarization. The p(2×2) (large green square) and c(2×2) (small green square) cells are marked. Arrows give direction and relative size of the spin polarization of the two Mn and Ni atoms within the unit cell.
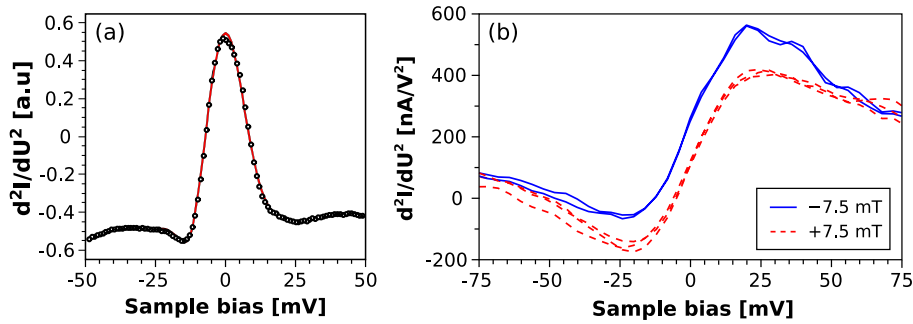

Figure 10. Inelastic d^2I/dU^2 spectrum recorded on Fe(001) at 4.3 K with (a) a non-magnetic tip and (b) with a Fe coated tip as function of the direction of a small applied magnetic field.

single atoms [50–52]. This new technique is based on inelastic scanning tunneling spectroscopy (ISTS). In ISTS, the tunneling electrons inelastically interact with one of the electrodes [53]. When the tunneling electrons have enough kinetic energy (eU) to excite an inelastic process, the tunneling current I is enhanced due to an increase of the number of final states. The onset of the inelastic scattering process creates a step in the differential conductivity dI/dU or a peak in the d^2I/dU^2. Inelastic excitations may occur in forward and backward tunneling direction, leading to peaks in d^2I/dU^2 with odd symmetry in U [53].

Figure 10(a) shows as an example the inelastic tunneling spectrum recorded on bulk Fe(001) with a non-magnetic tip. A clear peak at positive bias and a weak dip at negative bias indicate an inelastic excitation. The energy of the excitation is of the order of few meV and thus can be related to magnons or phonons. As the creation of a magnon by a hot electron reduces the total spin of the ferromagnet, the conservation of total angular momentum requires that the spin of the hot electron is changed from minority to majority during the

inelastic scattering event. Therefore, for positive sample bias U, magnons are created by hot minority electrons that are spin scattered. For negative U, magnons can only be created by majority electrons tunneling out of the ferromagnet leaving behind a hot majority hole that is filled by a minority electron due to an inelastic scattering event [49]. Inelastic phonon creation, however, does not obey these spin selection rules. Thus, inelastic magnon creation in ISTS can be told from inelastic phonon creation by verifying these spin selection rules. A straightforward verification can be done by using a spin-polarized STM tip as a source for spin-polarized electrons. Depending on the relative orientation of tip and sample spin polarization, the inelastic spectrum is expected to alter in case the excitations are magnons while the spectrum should not depend on the magnetization direction in case of phonons. Figure 10(b) shows the result of such an experiment. Again, the ISTS data was recorded on bulk Fe(001) but this time with a magnetic tip. By applying a small magnetic field of 7.5 mT, the soft magnetic Fe sample was switched while the hard magnetic STM tip was not switched. In agreement
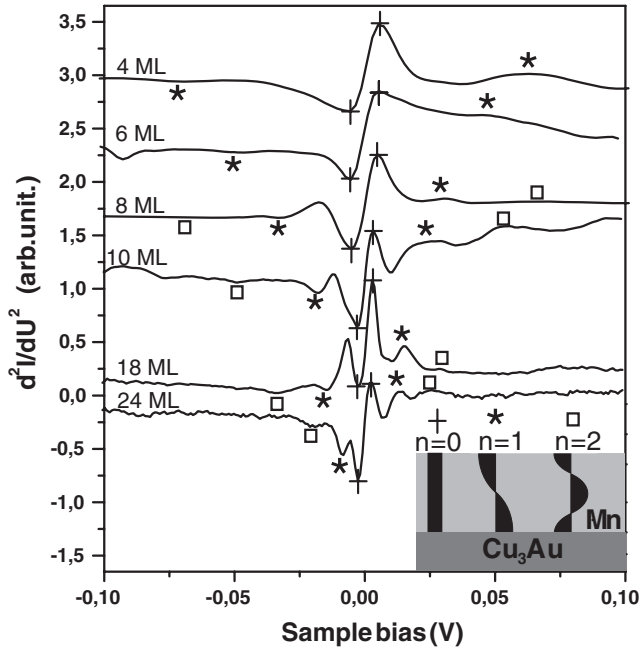
Figure 11. d^2I/dU^2 spectra of various thicknesses Mn thin films on Cu$_3$Au(001) taken at 5 K. The zero order (cross), first order (stars) and second order (squares) excitation peaks are marked in the figure. The excitations correspond to standing magnons in the thin films as sketched in the inset.

Figure 12. Spin wave dispersion of γ-Mn constructed from ISTS data. The bars on the data points represent the FWHM of the excitation peaks. The extrapolated neutron scattering data is from [56]. The fcc and fct Mn dispersions are given by the *ab initio* calculations. The inset plots the FWHM as a function of k together with the linear fit.

with magnon creation and in contrast to phonon creation, the inelastic spectra depend on the direction of the magnetic filed. Note that in this configuration magnons can also be created in the tip which explains the change of the spectra shape [50]. The excitation of magnons due to the local tunneling current allows to map magnon creation with the high lateral resolution of STM opening up a new research area that has been inaccessible with established scattering techniques like neutron scattering or Brillouin light scattering.

Beyond the lateral resolution, STM can also be used to determine the momenta and life times of magnons. The simple fcc γ-Mn can stabilized as ultra thin films on Cu$_3$Au(001) showing a layer-wise antiferromagnetic order [54]. While in bulk magnetic materials, magnons are free to travel in all three dimensions resulting in a continuous dispersion of the magnon energy E with the momentum k, in thin films magnons are confined normal to the film plane and standing magnons are formed. These standing magnons can be regarded as non-collinear magnetization oscillations that travel freely in the two dimensions of the film. Therefore, their dispersion relation is given by a series of spin wave branches quantized in k_z normal to the film plane and continuous in k_x and k_y in the film plane.

The d^2I/dU^2 spectra recorded on thin films of different thicknesses t are shown in figure 11. The peaks are antisymmetric with respect to zero bias voltage indicating an inelastic excitation. As both the substrate and the vacuum above the film are non-magnetic, the surface and interface spins of the antiferromagnetic layer are free to rotate such that magnons in the antiferromagnet are reflected with no phase shift at both interfaces. Thus the magnons can be classified by the order $n = 0, 1, 2, \ldots$ where n reflects the number of nodes
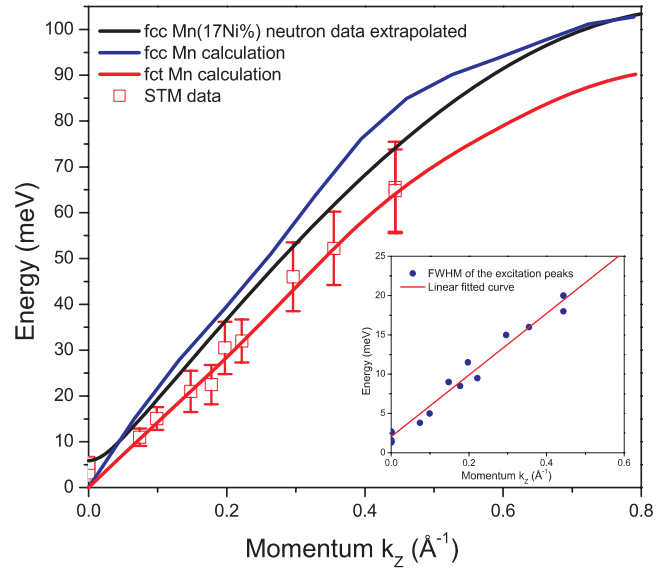
in the standing magnons as sketched in the inset of figure 11. In agreement with this simple quantization, we observe a series of excitation peaks in the inelastic spectra. The onset of every branch of standing magnons is observed as a peak in ISTS.

From the thickness t of the Mn layer and the order of the peak, we can compute the momentum k using a simple conversion $k_z = n\pi/t$. This way, both the energy E and the momentum k_z of the magnon can be obtained and the magnon dispersion can be measured as shown in figure 12. At low wavevector, the energy of the spin waves increase linearly as expected for antiferromagnetic magnons resulting in a magnon velocity of $v = 160 \pm 10$ meV Å/$\hbar$ in good agreement with Neutron scattering data of Ni stabilized bulk γ-Mn. A similarly good agreement is obtained when comparing our data with *ab initio* calculations of the magnon dispersion of fcc and fct bulk Mn [55].

Further more, we can measure the full width of half maximum (FWHM) of the excitation peaks from the spectra shown in figure 11. These give the damping of the magnons $\Gamma(k)$ which increases linearly with the energy in agreement with the viscous damping term of the Landau–Lifshitz–Gilbert equation.

6. Conclusion

In this review we summarized recent results of Sp-STM experiments that impressively show the capabilities of the technique to investigate non-collinear spin structures. Not only that the high resolution of Sp-STM allows to image the atomic spin structure for the first time, it also allows to obtain information on the direction of the spin polarization vector such that collinear and non-collinear states can be distinguished.

Ultimately, Sp-STM allows to investigate dynamic properties of magnets in form of their quantum mechanical excitations. All these recent achievements of Sp-STM are just the beginning and many new insights into the physics of magnetism on the atomic scale can be expected in the future.

Acknowledgments

References

[1] Zhu J G, Zheng Y and Prinz G A 2000 *J. Appl. Phys.* **87** 6668
[2] Stamm C, Marty F, Vaterlaus A, Weich V, Egger S, Maier U, Ramsperger U, Fuhrmann H and Pescia D 1998 *Science* **282** 449
[3] Kirk K J, Chapman J N and Wilkinson C D W 1997 *Appl. Phys. Lett.* **71** 539
[4] Bussmann K, Prinz G A, Cheng S F and Wang D 1999 *Appl. Phys. Lett.* **75** 2476
[5] Heisenberg W 1928 *Z. Phys.* **49** 619
[6] Yamada T, Kunitomi N, Nakai Y, Cox D E and Shirane G 1970 *J. Phys. Soc. Japan* **28** 615
[7] Lawson A C, Larson A C, Aronson M C, Johnson S, Fisk Z, Canfield P C, Thompson J D and Von Dreele R B 1994 *J. Appl. Phys.* **76** 7049
[8] Ohldag H, Scholl A, Nolting F, Anders S, Hillebrecht F U and Stöhr J 2001 *Phys. Rev. Lett.* **86** 2878
[9] Oepen H P, Steierl G and Kirschner J 2002 *J. Vac. Sci. Technol.* B **20** 2535
[10] Heinze S, Bode M, Kubetzka A, Pietzsch O, Nie X, Blügel S and Wiesendanger R 2000 *Science* **288** 1805
[11] Anderson P A 1973 *Mater. Res. Bull.* **8** 153
[12] Dzialoshinskii I E 1957 *Sov. Phys.—JETP* **5** 1259
[13] Moriya T 1960 *Phys. Rev.* **120** 91
[14] Tersoff J and Hamann D R 1983 *Phys. Rev. Lett.* **50** 1998
[15] Tersoff J and Hamann D R 1985 *Phys. Rev.* B **31** 805
[16] Binning G, Rohrer H, Gerber Ch and Weibel E 1982 *Appl. Phys. Lett.* **40** 178
[17] Binning G, Rohrer H, Gerber Ch and Weibel E 1982 *Phys. Rev. Lett.* **49** 57
[18] Jullière M 1975 *Phys. Lett.* A **54** 225
[19] Slonczewski J C 1989 *Phys. Rev.* B **39** 6995
[20] Miyazaki T and Tezuka N 1995 *J. Magn. Magn. Mater.* **139** L231
[21] Pierce D T 1988 *Phys. Scr.* **38** 291
[22] Wortmann D, Heinze S, Kurz P, Bihlmayer G and Blügel S 2001 *Phys. Rev. Lett.* **86** 4132
[23] Bode M, Vedmedenko E Y, von Bergmann K, Kubetzka A, Ferriani P, Heinze S and Wiesendanger R 2006 *Nat. Mater.* **5** 477
[24] Bode M, Heide M, von Bergmann K, Ferriani P, Heinze S, Bihlmayer G, Kubetzka A, Pietzsch O, Blügel S and Wiesendanger R 2007 *Nature* **447** 190
[25] Wulfhekel W and Kirschner J 1999 *Appl. Phys. Lett.* **75** 1944
[26] Schlickum U, Wulfhekel W and Kirschner J 2003 *Appl. Phys. Lett.* **83** 2016
[27] Wulfhekel W and Kirschner J 2007 *Annu. Rev. Mater. Res.* **37** 69
[28] Stamps R L 2000 *J. Phys. D: Appl. Phys.* **33** R247
[29] Kuch W, Chelaru L I, Offi F, Wang J, Kotsugi M and Kirschner J 2006 *Nat. Mater.* **5** 128
[30] Heinze S, Kurz P, Wortmann D, Bihlmayer G and Blügel S 2002 *Appl. Phys.* A **75** 25
[31] Krüger P, Taguchi M and Meza-Aguilar S 2000 *Phys. Rev.* B **61** 15277
[32] Kurz P, Bihlmayer G and Blügel S 2000 *J. Appl. Phys.* **87** 6101
[33] Spisak D and Hafner J 2000 *Phys. Rev.* B **61** 12728
[34] Kurz P, Bihlmayer G, Hirai K and Blügel S 2001 *Phys. Rev. Lett.* **86** 1106
[35] Gao C L, Wulfhekel W and Kirschner J 2008 *Phys. Rev. Lett.* **101** 267205
[36] Wachowiak A, Wiebe J, Bode M, Pietzche O, Morgenstern M and Wiesendanger R 2002 *Science* **298** 577
[37] Kim S K, Tian Y, Montesano M, Jona F and Marcus P M 1996 *Phys. Rev.* B **54** 5081
[38] Rader O, Gudat W, Schmitz D, Carbone C and Eberhardt W 1997 *Phys. Rev.* B **56** 5053
[39] Walker T G and Hopster H 1993 *Phys. Rev.* B **48** 3563
[40] Yamada T K, Bischoff M M J, Heijnen G M M, Mizoguchi T and van Kempen H 2003 *Phys. Rev. Lett.* **90** 056803
[41] Schlickum U, Janke-Gilman N, Wulfhekel W and Kirschner J 2004 *Phys. Rev. Lett.* **92** 107203
[42] Tulchinsky D A, Unguris J and Celotta R R 2000 *J. Magn. Magn. Mater.* **212** 91
[43] Gao C L, Schlickum U, Wulfhekel W and Kirschner J 2006 *Phys. Rev. Lett.* **98** 107203
[44] Kasper J S and Kouvel J S 1959 *J. Phys. Chem. Solids* **11** 231
[45] Tieg C, Kuch W, Wang S G and Kirschner J 2006 *Phys. Rev.* B **74** 094420
[46] Gao C L, Ernst A, Winkelmann A, Henk J, Wulfhekel W, Bruno P and Kirschner J 2008 *Phys. Rev. Lett.* **100** 237203
[47] Moodera J S, Nowak J and van de Veerdonk R J M 1998 *Phys. Rev. Lett.* **80** 2941
[48] Kubota H, Fukushima A, Yakushiji K, Nagahama T, Yuasa S, Ando K, Maehara H, Nagamine Y, Tsunekawa K and Djayaprawira D D 2008 *Nat. Phys.* **4** 37
[49] Balashov T, Takacs A F, Däne M, Ernst A, Bruno P and Wulfhekel W 2008 *Phys. Rev.* B **78** 174404
[50] Balashov T, Takács A F, Wulfhekel W and Kirschner J 2006 *Phys. Rev. Lett.* **97** 187201
[51] Hirjibehedin C F, Lin C Y, Otte A F, Ternes M, Lutz C P, Jones B A and Heinrich A J 2007 *Science* **317** 1199
[52] Hirjibehedin C F, Lutz C P and Heinrich A J 2006 *Science* **312** 1021
[53] Wolf E L 1985 *Principles of Electron Spectroscopy* (New York: Oxford University Press)
[54] Lin W C, Chen T Y, Lin L C, Wang B Y, Liao Y W, Song K J and Lin M T 2007 *Phys. Rev.* B **75** 054419
[55] Gao C L, Ernst A, Fischer G, Hergert W, Bruno P, Wulfhekel W and Kirschner J 2008 *Phys. Rev. Lett.* **101** 167201
[56] Jankowska-Kisielińska J, Mikke K and Milczarek J J 1995 *J. Magn. Magn. Mater.* **140–144** 1973